

Theoretical Studies on the Reaction Path Dynamics and Variational Transition-State Theory Rate Constants of the Hydrogen-Abstraction Reactions of the $\text{NH}(\text{X}^3\Sigma^-)$ Radical with Methane and Ethane

Zhen-Feng Xu,^{*,†,‡} Shen-Min Li,[†] Yong-Xue Yu,[†] Ze-Sheng Li,[†] and Chia-Chung Sun[†]

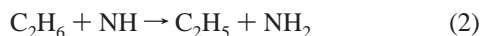
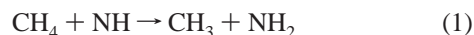
National Key Laboratory of Theoretical and Computational Chemistry, Institute of Theoretical Chemistry, Jilin University, Changchun 130023, People's Republic of China, and Department of Applied Chemistry, Beijing University of Chemical Technology, Beijing 100029, People's Republic of China

Received: November 20, 1998; In Final Form: April 20, 1999

The hydrogen-abstraction reactions of the radical $\text{NH}(\text{X}^3\Sigma^-)$ with methane and ethane have been studied by using ab initio molecular orbital theory and the canonical variational transition-state theory. The geometries of the reactants, transition states, and products were optimized at the UHF, UMP2, UMP4(sdq), and UQCISD levels of theory, and the forward and reverse reaction potential barriers were calculated accurately at the UQCISD(T)/6-311+G(3df,2p) and Gaussian 2 levels. The reaction paths were calculated by the intrinsic reaction coordinate theory at the UMP2/6-311G** level. The changes of the geometries and generalized normal-mode vibrational frequencies along the IRC were discussed. The energy profile along the IRC was further improved by the Gaussian 2 method. The forward and reverse reaction rate constants for the temperature range from 300 to 2000 K were evaluated by the conventional transition-state theory and the canonical variational transition-state theory with a small curvature tunneling correction. The theoretical rate constants of the forward and reverse reactions are all in good agreement with the experimental ones in the measured temperature range.

Introduction

The ground-state imidogen radical, $\text{NH}(\text{X}^3\Sigma^-)$, has received a great deal of attention in recent years because it is an important chain carrier in the combustion of energetic materials.¹ Some elementary reactions relative to the radical were investigated experimentally and theoretically. However, one has rarely paid attention to the hydrogen-abstraction reactions of imidogen radical with hydrocarbons. Recently, Rörig and Wagner² investigated the kind of reactions, including the reactions of NH with the saturated hydrocarbons and acetaldehyde, behind incident shock waves using narrow line-width absorption detection. They obtained experimentally the rate constants of these reactions. For both hydrogen-abstraction reactions of NH with methane and ethane,



the forward reaction rate constants obtained by Rörig and Wagner² are expressed as $k_1 = (9 \pm 3) \times 10^{13} \exp(-84 \pm 5) \text{ kJ mol}^{-1}/RT \text{ cm}^3 \text{ mol}^{-1} \text{ s}^{-1}$ for the temperature range from 1150 to 1500 K and $k_2 = (7 \pm 3) \times 10^{13} \exp(-70 \pm 5) \text{ kJ mol}^{-1}/RT \text{ cm}^3 \text{ mol}^{-1} \text{ s}^{-1}$ for the temperature range from 1010 to 1170 K, respectively, and the corresponding reverse reaction rate constant expressions are $k_{-1} = 10^{12} \exp(-34 \pm 10) \text{ kJ mol}^{-1}/RT \text{ cm}^3 \text{ mol}^{-1} \text{ s}^{-1}$ and $k_{-2} = 10^{12} \exp(-35 \pm 10) \text{ kJ mol}^{-1}/RT \text{ cm}^3 \text{ mol}^{-1} \text{ s}^{-1}$, respectively. To our knowledge, a theoretical investigation for these hydrogen-abstraction reactions has not been reported until now.

In the present paper, we apply ab initio electronic structure calculations and chemical reaction dynamical calculations to study the two hydrogen-abstraction reactions over a wide temperature range from 300 to 2000 K. The chemical reaction dynamical calculation based on canonical variational transition-state theory describes a chemical reaction by using ab initio electronic structure information only in the region of configuration space along the reaction path and provides a practical methodology for polyatomic reactions. In the second section of this paper, the theoretical methods of calculations are briefly summarized. The third section represents the locations of the stationary points and minimum energy path (MEP). The information about the electronic energy and the energy derivatives is calculated along the reaction coordinate. The theoretical rate constants based on the conventional transition-state theory and the canonical variational transition-state theory with a small curvature tunneling correction are presented. Several principal conclusions about this investigation are summarized in the final section.

Calculational Methods

Ab initio molecular orbital SCF calculations were carried out in the spin-unrestricted open-shell Hartree–Fock formalism³ (UHF) for reactions 1 and 2. The electronic correlation effect was calculated by using higher order post-SCF methods,^{3,4} including the frozen-core UMP2, UMP4(sdq), and UQCISD methods. The geometries of all the reactants, products, and transition states were optimized at the UHF, UMP2, UMP4(sdq), and UQCISD levels of theory for reaction 1 and at the UHF and UMP2 levels of theory for reaction 2. The transition state was further confirmed by computing the force constant

[†] Jilin University.

[‡] Beijing University of Chemical Technology.

matrix and characterized by only one imaginary vibrational mode. Furthermore, the single-point energy calculations at the Gaussian 2 theory^{5,6} (G2) and UQCISD(T)/6-311+G(3df,2p) level were performed at the frozen-core UMP2/6-311G** and UQCISD/6-311G** optimized geometries instead of at the full UMP2/6-31G* optimized geometries in the original G2 theory. The minimum energy paths (MEP) were calculated by the intrinsic reaction coordinate (IRC) theory⁷⁻⁹ at the UMP2/6-311G** level with a gradient step size of 0.05 amu^{1/2} bohr. Then, the UMP2 potential energy profiles were refined at the G2 theory. At some points along the IRC, we computed the matrix of force constants in order to do the following calculations of the canonical variational rate constants. All the electronic structure calculations were carried out by the GAUSSIAN 94 program.¹⁰

The canonical variational transition-state theory rate constant,¹¹⁻¹⁴ $k^{\text{CVT}}(T)$, at a fixed temperature (T) that minimized the generalized transition-state theory rate constant, $k^{\text{GT}}(T,s)$, with respect to the dividing surface at s is expressed as

$$k^{\text{CVT}}(T) = \min_s k^{\text{GT}}(T,s) \quad (3)$$

The generalized transition-state theory rate constant (k^{GT}) for T and a dividing surface at s is

$$k^{\text{GT}}(T,s) = \frac{\sigma Q^{\text{GT}}(T,s)}{\beta h Q^{\text{R}}(T)} \exp(-\beta V_{\text{MEP}}(s)) \quad (4)$$

In this equation, s is the location of the generalized transition state on the IRC; σ is the symmetry factor accounting for the possibility of two or more symmetry-related reaction paths; β equals $(k_{\text{B}}T)^{-1}$, where k_{B} is Boltzmann's constant and h is Planck's constant; $Q^{\text{R}}(T)$ is the reactant's partition function per unit volume, excluding symmetry numbers for rotation; $V_{\text{MEP}}(s)$ is the classical energy along the MEP overall zero of energy at the reactant; $Q^{\text{GT}}(T,s)$ is the partition function of generalized transition state at s with the local zero of energy at $V_{\text{MEP}}(s)$ and with all rotational symmetry numbers set to unity. For $s = 0$, eq 4 becomes the expression of the conventional transition-state theory (TST) rate constant.

For the forward directions of reactions 1 and 2, the symmetry numbers equal 12 and 6, respectively, and for the reverse directions of reactions 1 and 2, they are 12 and 2, respectively. The electronic degeneracies for calculating the partition functions are 1 for CH_4 and C_2H_6 , 2 for NH_2 , CH_3 , and C_2H_5 , 3 for NH , and 2 for both transition states. The electronic degeneracy of the generalized transition state is taken to be the same as the classical transition state corresponding to each reaction. In the calculations of the variational rate constants by the POLYRATE program,¹⁵ the gradient and Hessian grid step sizes are taken to be $0.005a_0$ and $0.02a_0$, respectively, so as to ensure the convergence of the calculated rate constants.

To include quantal effects for motion along the reaction coordinate, the CVT rate constant is multiplied by a ground-state transmission coefficient with the zero curvature tunneling (ZCT) approximation or the small curvature tunneling (SCT) approximation,¹⁶⁻¹⁹ which is denoted as the CVT/ZCT rate constant or the CVT/SCT rate constant. For tunneling calculations, the vibrationally adiabatic ground-state potential energy curve is expressed as

$$V_{\text{a}}^{\text{G}}(s) = V_{\text{MEP}}(s) + \text{ZPE}(s) \quad (5)$$

and for interpretative purposes, a version of the vibrationally

TABLE 1: Optimized Geometric Parameters of the Reactants and Products for Reaction 1^a

	CH ₄	NH	CH ₃	NH ₂ (C _{2v})	
	(T _d)		(D _{3h})	$R_{\text{N-H}}$	θ_{HNH}
UHF/6-31G	1.0821	1.0325	1.0716	1.0145	108.52
UHF/6-31G**	1.0830	1.0243	1.0728	1.0124	104.34
UHF/6-311G**	1.0838	1.0232	1.0735	1.0120	104.03
UMP2/6-31G	1.0956	1.0510	1.0833	1.0349	107.14
UMP2/6-31G**	1.0851	1.0352	1.0745	1.0243	103.32
UMP2/6-311G**	1.0904	1.0353	1.0791	1.0252	102.00
UMP4(sdq)/6-311G**	1.0925	1.0404	1.0818	1.0281	101.81
UQCISD/6-311G**	1.0932	1.0425	1.0831	1.0294	101.80
expt ²⁰	1.094	1.035	1.079	1.024	103.3

^a Bond lengths in Å, bond angles in deg.

adiabatic ground-state potential energy curve is given by

$$\Delta V_{\text{a}}^{\text{G}}(s) = V_{\text{a}}^{\text{G}}(s) - \text{ZPE}(\text{R}) \quad (6)$$

Here R represents the reactants. The POLYRATE program¹⁵ was employed to calculate the theoretical rate constants.

Results and Discussion

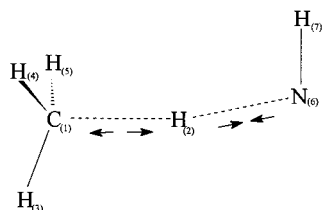
A. Reaction 1: $\text{CH}_4 + \text{NH} \rightarrow \text{CH}_3 + \text{NH}_2$. The optimized geometries for the reactants and products of reaction 1 are given in Table 1. At the UHF level of theory, the bond lengths of the species are generally shorter than the experimental values, but by at most 1.1%. However, at the UMP2, UMP4(sdq), and UQCISD levels of theory with the 6-311G** basis set, the bond lengths agree within 0.7% with the experimental data. It is shown that the electron-correlated effect is very important to the geometrical optimization of these species. Also, from the UHF and UMP2 results at three basis sets, we can find that the large basis set with polarization functions gives better geometric parameters close to the experimental values. Therefore, it is expected that the UMP2/6-311G** method is feasible to calculate the reaction path.

The transition-state structures optimized at four levels of theory for the hydrogen-abstraction reaction (1), are listed in Table 2. The transition state of this reaction is of C_s symmetry and is located in the potential energy surface of the ³A'' electronic state. Its structure is staggered, and the N-H fragment is trans with respect to one of the C-H bonds of the methyl group. Because the expectation values of S² (where S denotes electron spin angular momentum) of the transition state in spin-unrestricted wave functions are no more than 2.058, where 2.000 is the correct value for a pure triplet, the spin contamination is not considered severe. The atom numbering of the transition-state structure and the imaginary vibrational mode are drawn in Figure 1. From Table 2, it can be easily seen that the geometric parameters of the transition state at the UMP2/6-311G** level of theory are in good agreement with those at the UMP4(sdq)/6-311G** and UQCISD/6-311G** levels of theory. Also, the polarization functions used had an obvious effect on the transition-state structure. The interatomic distance of C₍₁₎ and H₍₂₎ at the 6-31G** basis set is at least 0.03 Å shorter than that at the 6-31G basis set, and the interatomic distance of H₍₂₎ and N₍₆₎ at the 6-31G** basis set is about 0.01 Å longer than that at the 6-31G basis set. Comparing the geometric parameters of the transition state with those of reactants and products, one can find that at the UMP2 and UQCISD levels of theory with the 6-311G** basis set, the breaking C₍₁₎-H₍₂₎ bond length is elongated by about 30% to the C-H bond length of CH₄ and the making H₍₂₎-N₍₆₎ bond length is about 15%

TABLE 2: Optimized Transition-State Structures (C_s) for Reaction 1^a

	UHF			UMP2			UMP4(sdq)	UQCISD
	6-31G	6-31G**	6-311G**	6-31G	6-31G**	6-311G**	6-311G**	6-311G**
C ₍₁₎ –H ₍₂₎	1.4447	1.4131	1.4104	1.4394	1.3993	1.3986	1.4149	1.4212
C ₍₁₎ –H ₍₃₎	1.0769	1.0786	1.0792	1.0911	1.0820	1.0867	1.0886	1.0893
C ₍₁₎ –H ₍₄₎	1.0773	1.0791	1.0796	1.0912	1.0822	1.0866	1.0887	1.0894
H ₍₂₎ –N ₍₆₎	1.2091	1.2184	1.2186	1.1942	1.1833	1.1830	1.1874	1.1923
N ₍₆₎ –H ₍₇₎	1.0244	1.0189	1.0180	1.0445	1.0315	1.0321	1.0349	1.0365
∠H ₍₃₎ C ₍₁₎ H ₍₂₎	100.77	102.29	102.36	100.67	101.79	101.71	101.82	101.77
∠H ₍₄₎ C ₍₁₎ H ₍₂₎	104.51	105.11	105.08	105.24	105.33	105.16	104.89	104.92
∠H ₍₄₎ C ₍₁₎ H ₍₃₎	114.86	114.20	114.22	114.58	114.23	114.39	114.45	114.49
∠N ₍₆₎ H ₍₂₎ C ₍₁₎	175.14	175.88	173.93	170.44	171.53	169.31	169.86	169.84
∠H ₍₇₎ N ₍₆₎ H ₍₂₎	103.66	100.10	99.70	104.07	99.85	98.74	98.55	98.52
∠H ₍₄₎ C ₍₁₎ H ₍₂₎ H ₍₃₎	119.42	119.56	119.60	119.34	119.47	119.54	119.58	119.59

^a Lengths in Å, bond angles, and dihedral angles in deg.

**Figure 1.** Transition-state structure of reaction 1 and its imaginary vibrational mode.

longer than the N–H bond length in NH₂. It means that the transition-state structure is more product-like than reactant-like. In addition, the C₍₁₎–H₍₂₎–N₍₆₎ angle at the transferred H₍₂₎ is bent by about 10° from the linear structure at the three levels of theory.

Table 3 lists the vibrational frequencies of the transition state optimized at the different levels of theory for the hydrogen-abstraction reaction (1). From this table, we can find that the imaginary vibrational frequency at the UMP2 level is about 800 cm⁻¹ less than that at the UHF level and about 70 cm⁻¹ larger than that at the UQCISD level with the 6-311G** basis set. However, although it is much less than the UHF imaginary frequency and very close to the UQCISD imaginary frequency, the UMP2 imaginary frequency is still quite large, about 2000 cm⁻¹. Because the imaginary frequency governs the width of the classical potential energy barrier during the reaction process, it plays an important role in the tunneling calculations, especially when the imaginary frequency is large. So we expect that the tunneling effect should be important to the rate constant calculation of the reaction at lower temperatures.

The potential energy barriers and enthalpy of reaction 1 are listed in Table 4. As mentioned above, the differences in energies also depend on the electronic correlation and basis set used. At the UHF level of theory, the potential barrier heights and enthalpy of reaction are all overestimated, and the enthalpy of reaction at UHF/6-311G** is 29 kJ/mol greater than the value, 49.4 kJ/mol, in ref 2. However, including the electron correlation lowers the UHF barrier height by more than 33% at the UMP2 method, while it decreases the UHF enthalpy of reaction about 13 kJ/mol. Also, one can find that the forward barrier height and the enthalpy of reaction at UMP2/6-311G** are almost the same as those at UQCISD/6-311G** and slightly lower than those at UMP4/6-311G**. Single-point energy calculations using G2 theory at the UMP2/6-311G**- and UQCISD/6-311G**-optimized structures further decrease the forward and reverse potential barrier heights to about 90 and 40 kJ/mol, respectively, and lessen the enthalpy of reaction to about 52 kJ/mol, which is only about 3 kJ/mol greater than the value in ref 2. It can be apparently seen from Table 4 that the theoretical

results with the G2 theory agree excellently with the most accurate ones at the UQCISD(T)/6-311+G(3df,2p) level of theory.

The minimum energy path of reaction 1 based on the intrinsic reaction coordinate theory has been traced at the UMP2 level of theory with the 6-311G** basis set. The potential energy profile was further improved with G2 theory. Figure 2 gives the classical potential energy curve ($V_{\text{MEP}}(s)$) and the ground-state vibrationally adiabatic potential energy curve ($\Delta V_a^G(s)$) as a function of the intrinsic reaction coordinate (s) at the G2//UMP2/6-311G** level of theory. It can be seen that the ground-state vibrationally adiabatic potential energy curve is below the classical potential energy curve near the transition state and the maximum positions of the two potential energy curves are almost the same. Figure 3 describes the changes of the interatomic distances along the IRC. It appears that the H₍₂₎–N₍₆₎ distance shortens linearly along s and reaches the bond length of NH₂ at about $s = 0.5 \text{ amu}^{1/2} \text{ bohr}$, while the C₍₁₎–H₍₂₎ bond length elongates linearly after about $s = -0.6 \text{ amu}^{1/2} \text{ bohr}$ and tends to infinity. Other bond lengths have almost no variation during the reaction process. It is thus evident that the hydrogen abstraction from C₍₁₎ to N₍₆₎ essentially takes place in the region of $s = -0.6$ – $0.5 \text{ amu}^{1/2} \text{ bohr}$. This means that the region of the hydrogen-abstraction reaction path represents the main interaction of the reaction process.

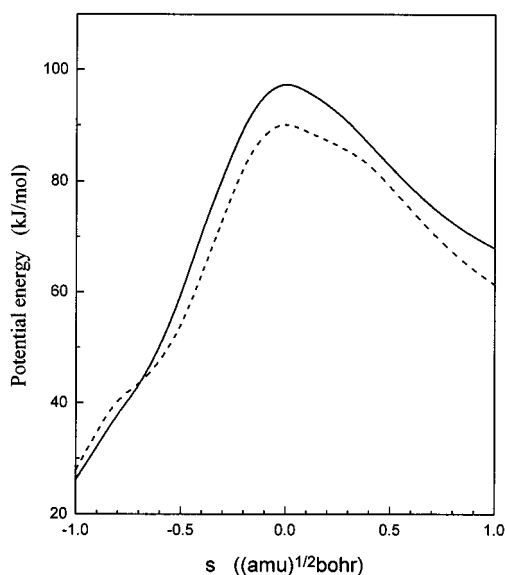
The variation of the generalized normal-mode vibrational frequencies of reaction 1 along the IRC is drawn in Figure 4. In the negative limit of s ($s = -\infty$), the generalized normal-mode frequencies correspond to the CH₄ + NH reactants, and in the positive limit of s ($s = +\infty$), the generalized normal-mode frequencies are associated with the CH₃ + NH₂ products. The four lowest frequencies of these vibrational modes are varied corresponding to free rotations and translations of the reactants that evolve to vibrations. These frequencies appear near the transition state and tend toward zero in the directions of the reactants and the products. Modes 5, 8, 9, and 11–13 evolve to the CH₃ vibration and modes 7, 10, and 14 to the NH₂ vibration as the reaction proceeds. Of these vibrational modes, the frequency curve of mode 10 has the dramatic variation in the course of the reaction, and this mode connects the C₍₁₎–H₍₂₎ stretching vibration of CH₄ with the H₍₂₎–N₍₆₎ stretching vibration of NH₂. By analyzing the vibrational displacement vector of mode 10 along the IRC, we find the vibrational transformation from the C₍₁₎–H₍₂₎ stretching to the H₍₂₎–N₍₆₎ stretching takes place in the range $[-0.4, 0.1]$ of s . Before the point of about $s = -0.4 \text{ amu}^{1/2} \text{ bohr}$, there is only the C₍₁₎–H₍₂₎ stretching vibration, and after a point of about $s = 0.1 \text{ amu}^{1/2} \text{ bohr}$, only the H₍₂₎–N₍₆₎ stretching vibration exists. Between -0.4 and $0.1 \text{ amu}^{1/2} \text{ bohr}$ on the IRC, the approximate

TABLE 3: Transition State Harmonic Vibrational Frequencies (cm^{-1}) and Zero-Point Vibrational Energies (ZPE, kJ/mol) for Reaction 1

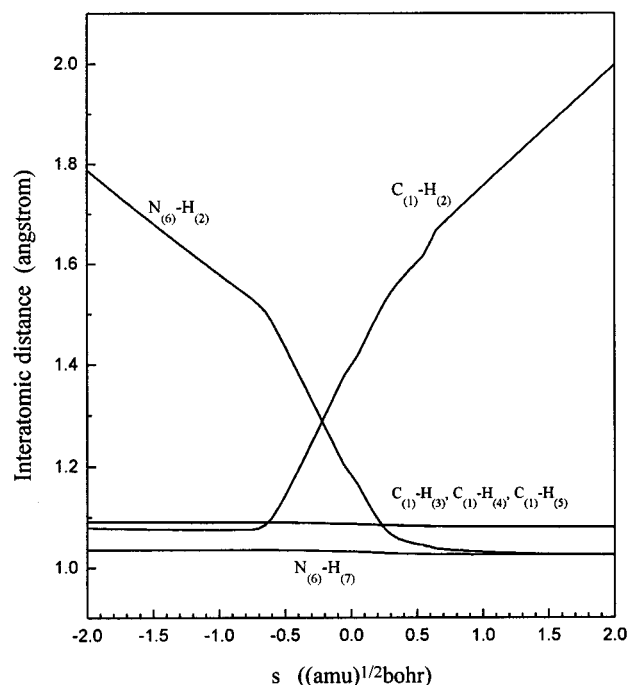
mode	UHF			UMP2			UMP4(sdq)	UQCISD
	6-31G	6-31G**	6-311G**	6-31G	6-31G**	6-311G**	6-311G**	6-311G**
F(a')	i2692	i2779	i2775	i2142	i2030	i1977	i1959	i1906
1(a'')	44	51	59	60	72	80	90	85
2(a')	380	378	375	371	366	373	368	361
3(a'')	454	437	438	443	424	425	429	421
4(a')	509	856	530	568	600	598	585	567
5(a')	867	857	866	812	830	824	815	805
6(a'')	1206	1207	1195	1179	1178	1168	1144	1127
7(a')	1256	1250	1237	1225	1222	1193	1182	1167
8(a')	1555	1517	1500	1505	1483	1449	1447	1442
9(a'')	1578	1561	1546	1509	1501	1462	1460	1456
10(a')	1584	1568	1552	1532	1517	1492	1492	1482
11(a'')	3233	3222	3194	3111	3178	3118	3099	3088
12(a'')	3379	3358	3327	3265	3337	3274	3244	3230
13(a')	3385	3364	3332	3267	3341	3276	3248	3234
14(a')	3486	3580	3565	3302	3453	3424	3382	3351
ZPE	137.1	137.0	135.9	132.5	134.6	132.5	131.5	130.5

TABLE 4: Forward and Reverse Reaction Barriers (V^\ddagger) and Reaction Enthalpy (ΔH_{298}°) (in kJ/mol) for Reaction 1

	forward reaction		reverse reaction		ΔH_{298}°
	V^\ddagger	$V^\ddagger + \Delta\text{ZPE}$	V^\ddagger	$V^\ddagger + \Delta\text{ZPE}$	
UHF/6-31G	180.9	172.0	66.0	67.9	105.9
UHF/6-31G**	169.0	160.4	76.9	79.2	83.3
UHF/6-311G**	166.8	158.4	79.6	81.7	78.8
UMP2/6-31G	140.6	133.1	43.9	46.4	88.4
UMP2/6-31G**	121.5	113.5	43.0	45.2	70.3
UMP2/6-311G**	113.1	106.0	40.6	42.9	65.0
UMP4(sdq)/6-311G**	117.2	110.2	41.1	43.6	68.5
UQCISD/6-311G**	113.5	106.1	38.3	40.5	67.5
UQCISD(T)/6-311+G(3df,2p)/UMP2/6-311G**	97.9	90.7	37.7	41.8	52.6
UQCISD(T)/6-311+G(3df,2p)/UQCISD/6-311G**	97.3	89.9	37.1	39.3	52.5
G2/UMP2/6-311G**		91.0		40.2	52.4
G2/UQCISD/6-311G**		89.9		39.6	52.1

**Figure 2.** Classical potential energy curve ($V_{\text{MEP}}(s)$, solid line) and vibrationally adiabatic ground-state potential energy curve ($\Delta V_a^G(s)$, dashed line) of reaction 1 as a function of s at the G2//UMP2/6-311G** level of theory.

symmetric stretching vibration appears in the $\text{C}_{(1)}-\text{H}_{(2)}-\text{N}_{(6)}$ structure. Namely, in this interval, the transformation of the vibrational vector of mode 10 from the $\text{C}_{(1)}-\text{H}_{(2)}$ stretching vibration to the $\text{H}_{(2)}-\text{N}_{(6)}$ stretching vibration is finished. It means that mode 10 represents mainly the course of the hydrogen-abstraction reaction and can be referred to as the “key mode”. From Figure 4, it can be seen that mode 10 undergoes

**Figure 3.** Changes of the bond lengths (in Å) of reaction 1 as a function of s .

a deep frequency valley of about 2000 cm^{-1} and the width of the frequency valley is the region from about $s = -0.7$ to $0.8\text{ amu}^{1/2}\text{ bohr}$ on the IRC. The position of the frequency valley looks like the region of the main geometric changes. The frequency variation of mode 10 results in the ground-state

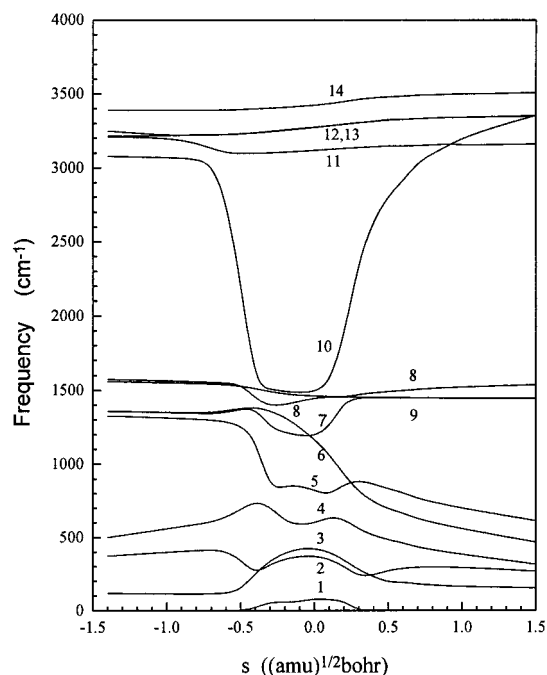


Figure 4. Generalized normal-mode vibrational frequencies of reaction 1 as a function of s .

vibrationally adiabatic potential energy being lower than the classical potential energy at about $s > -0.7 \text{ amu}^{1/2} \text{ bohr}$.

Table 5 lists the conventional and canonical variational transition-state theory rate constants with a small curvature tunneling correction for reaction 1 in a wide temperature range from 300 to 2000 K at the G2//UMP2/6-311G** level. The location of the variational transition state of the forward reaction ranges from $0.0054 \text{ amu}^{1/2} \text{ bohr}$ at 500 K to $0.0061 \text{ amu}^{1/2} \text{ bohr}$ at 2000 K, and that of the reverse reaction distributes from $0.0043 \text{ amu}^{1/2} \text{ bohr}$ at 500 K to $0.0051 \text{ amu}^{1/2} \text{ bohr}$ at 2000 K. At 2000 K, the variational transition state is at a location where the potential energy is 0.008 kJ/mol below the classical transition state. This illustrates roughly that the variational effect is small for the forward and reverse reactions, which is fully testified by the comparison of the TST and CVT rate constants in Table 5. Besides, the tunneling and curvature effects of the reaction path have a greater influence on the rate constants in the lower temperature range, particularly close to room temperature.

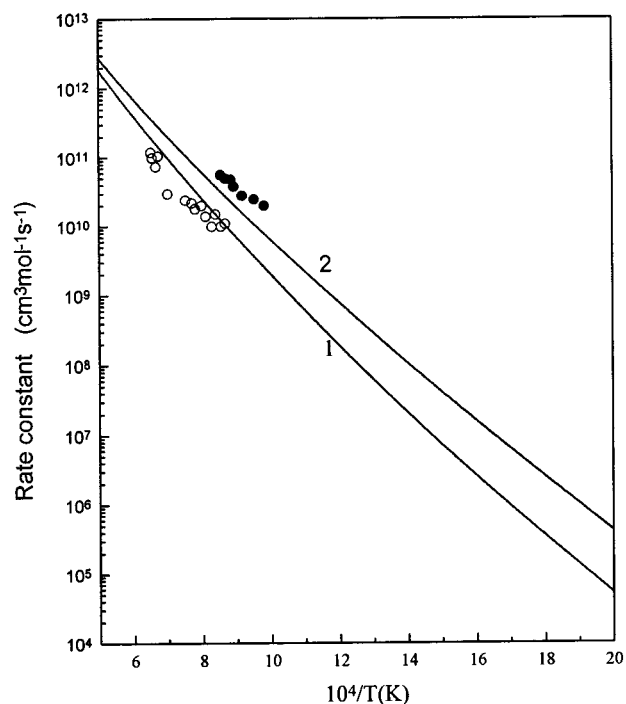


Figure 5. Plot of the CVT/SCT and experimental rate constants ($\text{cm}^3 \text{ mol}^{-1} \text{ s}^{-1}$) of the forward reaction along the reciprocal of temperature T . Solid line 1, CVT/SCT rate constants of reaction 1; solid line 2, CVT/SCT rate constants of reaction 2; \circ , experimental rate constants of reaction 1; \bullet , experimental rate constants of reaction 2.

For the forward reaction, the CVT/SCT rate constants agree very well with the experimental data over the measured temperature range from 1100 to 1500 K, shown in Figure 5. The CVT/SCT rate constants over the temperature range from 1300 to 1500 K are slightly larger than the experimental ones, and the deviations between the CVT/SCT and the experimental rate constants are very small. So the CVT/SCT method can give us quite reliable results for the hydrogen-abstraction reaction in a wider temperature range. From Table 5, we think reasonably that reaction 1 will happen very slowly at room temperature because the calculated rate constant is only $1.27 \text{ cm}^3 \text{ mol}^{-1} \text{ s}^{-1}$ at 300 K.

For the reverse reaction, the CVT/SCT rate constants in the temperature range from 1100 to 1500 K are a factor of about

TABLE 5: Forward and Reverse Reaction Rate Constants ($\text{cm}^3 \text{ mol}^{-1} \text{ s}^{-1}$) of Reaction 1 at the G2//UMP2/6-311G Level**

T, K	forward reaction					reverse reaction				
	TST	CVT	CVT/ZCT	CVT/SCT	expt ^a	TST	CVT	CVT/ZCT	CVT/SCT	expt ^a
300	2.54×10^{-3}	2.54×10^{-3}	9.68×10^{-3}	1.27		2.21×10^5	2.20×10^5	8.40×10^5	5.06×10^7	
400	2.61×10	2.61×10	5.40×10	7.17×10^2		1.11×10^7	1.11×10^7	2.34×10^7	1.63×10^8	
500	7.59×10^3	7.59×10^3	1.20×10^4	5.29×10^4		1.27×10^8	1.27×10^8	2.03×10^8	5.67×10^8	
600	3.66×10^5	3.66×10^5	5.01×10^5	1.28×10^6		6.93×10^8	6.87×10^8	9.57×10^8	1.77×10^9	
700	6.32×10^6	6.26×10^6	7.91×10^6	1.50×10^7		2.46×10^9	2.46×10^9	3.13×10^9	4.70×10^9	
800	5.63×10^7	5.62×10^7	6.69×10^7	1.07×10^8		6.68×10^9	6.68×10^9	8.06×10^9	1.08×10^{10}	
900	3.24×10^8	3.23×10^8	3.70×10^8	5.26×10^8		1.53×10^{10}	1.53×10^{10}	1.77×10^{10}	2.20×10^{10}	
1000	1.36×10^9	1.35×10^9	1.51×10^9	2.00×10^9		3.07×10^{10}	3.06×10^{10}	3.44×10^{10}	4.09×10^{10}	
1100	4.53×10^9	4.52×10^9	4.94×10^9	6.20×10^9	9.23×10^9	5.57×10^{10}	5.56×10^{10}	6.13×10^{10}	7.05×10^{10}	2.43×10^{10}
1200	1.26×10^{10}	1.26×10^{10}	1.36×10^{10}	1.63×10^{10}	1.98×10^{10}	9.39×10^{10}	9.39×10^{10}	1.02×10^{11}	1.14×10^{11}	3.31×10^{10}
1300	3.07×10^{10}	3.07×10^{10}	3.27×10^{10}	3.81×10^{10}	3.79×10^{10}	1.49×10^{11}	1.49×10^{11}	1.60×10^{11}	1.76×10^{11}	4.30×10^{10}
1400	6.68×10^{10}	6.68×10^{10}	7.05×10^{10}	8.07×10^{10}	6.61×10^{10}	2.27×10^{11}	2.26×10^{11}	2.41×10^{11}	2.61×10^{11}	5.39×10^{10}
1500	1.33×10^{11}	1.33×10^{11}	1.39×10^{11}	1.56×10^{11}	1.07×10^{11}	3.31×10^{11}	3.31×10^{11}	3.48×10^{11}	3.74×10^{11}	6.55×10^{10}
1600	2.46×10^{11}	2.46×10^{11}	2.56×10^{11}	2.83×10^{11}		4.67×10^{11}	4.66×10^{11}	4.88×10^{11}	5.20×10^{11}	
1700	4.29×10^{11}	4.28×10^{11}	4.43×10^{11}	4.84×10^{11}		6.38×10^{11}	6.38×10^{11}	6.66×10^{11}	7.05×10^{11}	
1800	7.11×10^{11}	7.05×10^{11}	7.28×10^{11}	7.89×10^{11}		8.55×10^{11}	8.55×10^{11}	8.88×10^{11}	9.33×10^{11}	
1900	1.12×10^{12}	1.11×10^{12}	1.15×10^{12}	1.23×10^{12}		1.13×10^{12}	1.12×10^{12}	1.16×10^{12}	1.21×10^{12}	
2000	1.70×10^{12}	1.69×10^{12}	1.74×10^{12}	1.85×10^{12}		1.45×10^{12}	1.45×10^{12}	1.49×10^{12}	1.55×10^{12}	

^a Experimental values calculated by the rate constant expression in ref 2.

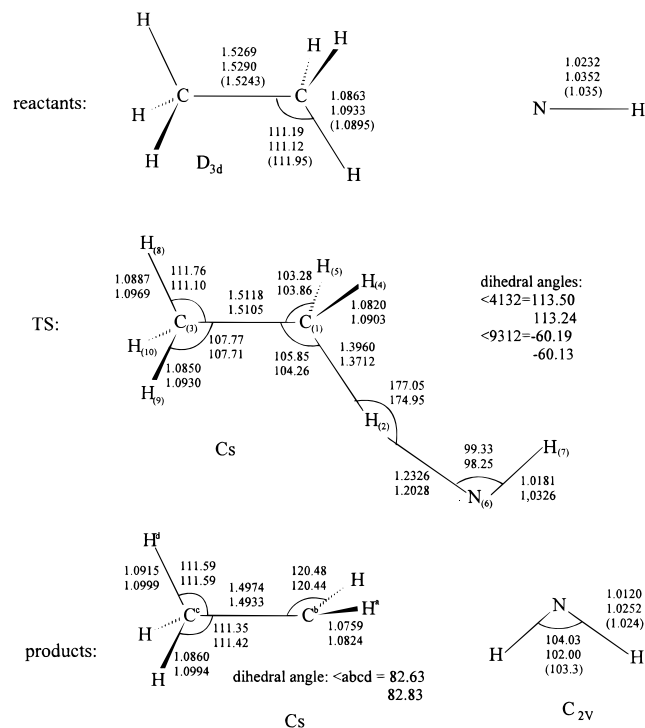


Figure 6. Optimized geometries (bond lengths in angstroms and bond angles in degrees) of C_2H_6 , C_2H_5 , and transition state of reaction 2. Top line is the value at UHF/6-311G**; second line is the value at UMP2/6-311G**; experimental value is in parentheses (ref 21 for C_2H_6).

3–5 greater than the experimental values and agree better with the upper limit of the uncertainty of the experimentally estimated data. This shows that the reverse reaction rate constants calculated by the CVT/SCT theory at the G2//UMP2/6-311G** level are credible for the wide temperature range from 300 to 2000 K. Compared with the forward rate constants, the reverse reaction may take place much easier below about 1200 K. In the temperature range 1300–1700 K, the rate constants of the reverse reaction are 2–4 times larger than those of the forward reaction. However, above 1800 K, the rate constants of the reverse and forward reactions are almost equal.

B. Reaction 2: $\text{C}_2\text{H}_6 + \text{NH} \rightarrow \text{C}_2\text{H}_5 + \text{NH}_2$. Because of the similarity of reaction 2 to reaction 1, we have reason to choose the UHF and UMP2 levels of theory with the 6-311G** basis set to optimize the geometries of the C_2H_6 , C_2H_5 , and transition state of reaction 2. The optimized geometries are shown in Figure 6. The transition state of reaction 2 is of C_s symmetry and is located in the potential energy surface of the $^3\text{A}''$ electronic state. The expectation value of S^2 of the transition state is no more than 2.0534. From Figure 6, it can be seen that the electron correlation plays an important role in the mainly changed configuration, $\text{C}_{(1)}-\text{H}_{(2)}-\text{N}_{(6)}$, of the transition-state structure. Comparing the geometric parameters of the transition state with the equilibrium structures of C_2H_6 and NH_2 , one can find that at the UMP2 level the breaking $\text{C}_{(1)}-\text{H}_{(2)}$ bond length is elongated by about 25.4% to the C–H bond length of C_2H_6 and the making $\text{H}_{(2)}-\text{N}_{(6)}$ bond length is about 17.3% longer than the N–H bond length of NH_2 . That is, the transition-state structure is more product-like than reactant-like, too. Table 6 lists the vibrational frequencies of the C_2H_6 , C_2H_5 , and transition state of reaction 2 at the UMP2/6-311G** level. For the transition state, we can find that there is a quite large imaginary frequency just like in reaction 1. So the tunneling effect for the dynamical property of reaction 2 should not be ignored in the lower temperature range, too. The forward and reverse potential

TABLE 6: Harmonic Vibrational Frequencies (cm^{-1}) and Zero-Point Energies (kJ/mol) of the C_2H_6 , C_2H_5 , and Transition State of Reaction 2 at the UMP2/6-311G Level**

	C_2H_6	transition state		C_2H_5
a_{1g}	3081	a' 3417	a'' 3221	a' 3206
a_{1g}	1448	a' 3145	a'' 3171	a' 3121
a_{1g}	1034	a' 3064	a'' 3130	a' 3037
a_{1u}	332	a' 1512	a'' 1510	a' 1511
a_{2u}	3081	a' 1491	a'' 1256	a' 1496
a_{2u}	1420	a' 1462	a'' 1209	a' 1421
e_g	3155	a' 1422	a'' 840	a' 1090
e_g	1524	a' 1218	a'' 476	a' 999
e_g	1241	a' 1080	a'' 171	a' 460
e_u	3177	a' 933	a'' 53	a'' 3318
e_u	1526	a' 739		a'' 3167
e_u	833	a' 506		a'' 1510
		a' 132		a'' 1218
		a' 2042i		a'' 820
				a'' 164
ZPE (kJ/mol)	199.3	210.4		158.8

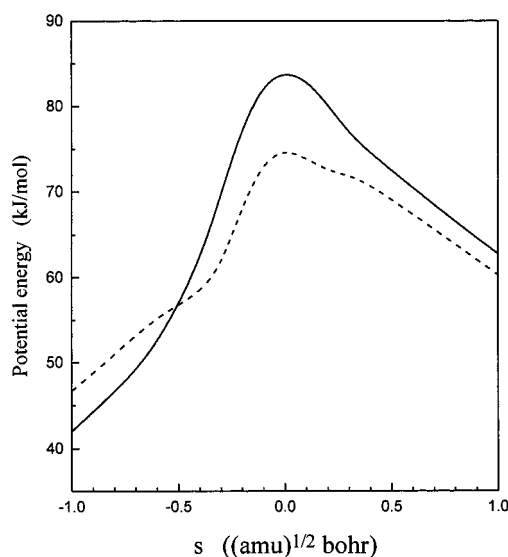


Figure 7. Classical potential energy curve ($V_{\text{MEP}}(s)$, solid line) and vibrationally adiabatic ground-state potential energy curve ($\Delta V_a^G(s)$, dashed line) of reaction 2 at the G2//UMP2/6-311G** level.

energy barriers and the enthalpy of reaction 2 are listed in Table 7. These data are overestimated greatly at the UHF level and decreased obviously at the UMP2 level. At the G2//UMP2/6-311G** level, the forward and reverse reaction barriers and enthalpy of reaction 2 are 74.9, 38.9, and 38.4 kJ/mol, respectively. The calculated reaction enthalpy is only 4.7 kJ/mol greater than the value, 33.7 kJ/mol, in ref 2.

The classical potential energy curve ($V_{\text{MEP}}(s)$) and vibrationally adiabatic ground-state potential energy curve ($\Delta V_a^G(s)$) of reaction 2 are drawn in Figure 7. Because of the zero-point vibrational energy, $\Delta V_a^G(s)$ is obviously lower than $V_{\text{MEP}}(s)$ at about $s > -0.5$ amu^{1/2} bohr. Figure 8 describes the changes of the interatomic distances along the IRC. It can be seen that in the hydrogen-abstraction reaction process, the breaking of the $\text{C}_{(1)}-\text{H}_{(2)}$ bond and the forming of the $\text{H}_{(2)}-\text{N}_{(6)}$ bond essentially take place in the region of $s = -0.6-0.5$ amu^{1/2} bohr. The generalized normal-mode vibrational frequencies along the IRC are given in Figure 9. It can be easily seen that the frequency curve of mode 17 has the dramatic variation in the course of the reaction and this mode is the “key mode” that connects the $\text{C}_{(1)}-\text{H}_{(2)}$ stretching vibration of C_2H_6 with the $\text{H}_{(2)}-\text{N}_{(6)}$ stretching vibration of NH_2 . Analyzing the vibrational displacement vector of mode 17 along the IRC shows

TABLE 7: Forward and Reverse Reaction Potential Barriers (V^\ddagger), and Enthalpy (ΔH_{298}°) of Reaction 2 (in kJ/mol)

	forward reaction		reverse reaction		ΔH_{298}°
	V^\ddagger	$V^\ddagger + \Delta ZPE$	V^\ddagger	$V^\ddagger + \Delta ZPE$	
UHF/6-311G**	158.2	148.4	81.8	82.2	68.7
UMP2/6-311G**	101.2	92.0	39.3	39.8	54.6
UQCISD(T)/6-311G**//UMP2/6-311G**	88.2	79.0	32.1	32.6	48.9
G2//UMP2/6-311G**		74.9		38.9	38.4

TABLE 8: Forward and Reverse Reaction Rate Constants ($\text{cm}^3 \text{mol}^{-1} \text{s}^{-1}$) of Reaction 2 at the G2//UMP2/6-311G Level**

<i>T</i> , K	forward reaction					reverse reaction				
	TST	CVT	CVT/ZCT	CVT/SCT	expt ^a	TST	CVT	CVT/ZCT	CVT/SCT	expt ^a
300	0.62	0.52	2.45	8.49		4.93×10^4	4.29×10^4	1.93×10^5	5.20×10^5	
400	1.57×10^3	1.27×10^3	2.99×10^3	6.08×10^3		2.54×10^6	2.13×10^6	4.83×10^6	8.37×10^6	
500	1.96×10^5	1.57×10^5	2.67×10^5	4.22×10^5		2.96×10^7	2.42×10^7	4.00×10^7	5.68×10^7	
600	5.44×10^6	4.29×10^6	6.11×10^6	8.43×10^6		1.64×10^8	1.32×10^8	1.84×10^8	2.34×10^8	
700	6.26×10^7	4.91×10^7	6.29×10^7	7.95×10^7		5.98×10^8	4.74×10^8	5.94×10^8	7.11×10^8	
800	4.17×10^8	3.24×10^8	3.87×10^8	4.65×10^8		1.66×10^9	1.30×10^9	1.53×10^9	1.75×10^9	
900	1.90×10^9	1.47×10^9	1.68×10^9	1.93×10^9		3.84×10^9	2.98×10^9	3.35×10^9	3.73×10^9	
1000	6.62×10^9	5.09×10^9	5.63×10^9	6.32×10^9	1.54×10^{10}	7.77×10^9	5.99×10^9	6.53×10^9	7.11×10^9	1.48×10^{10}
1100	1.90×10^{10}	1.45×10^{10}	1.57×10^{10}	1.72×10^{10}	3.32×10^{10}	1.43×10^{10}	1.10×10^{10}	1.17×10^{10}	1.25×10^{10}	2.18×10^{10}
1200	4.67×10^{10}	3.55×10^{10}	3.77×10^{10}	4.09×10^{10}	6.28×10^{10}	2.43×10^{10}	1.85×10^{10}	1.94×10^{10}	2.07×10^{10}	2.99×10^{10}
1300	1.02×10^{11}	7.71×10^{10}	8.09×10^{10}	8.67×10^{10}		3.90×10^{10}	2.96×10^{10}	3.06×10^{10}	3.23×10^{10}	
1400	2.03×10^{11}	1.53×10^{11}	1.59×10^{11}	1.69×10^{11}		5.94×10^{10}	4.50×10^{10}	4.61×10^{10}	4.82×10^{10}	
1500	3.73×10^{11}	2.81×10^{11}	2.89×10^{11}	3.04×10^{11}		8.73×10^{10}	6.56×10^{10}	6.69×10^{10}	6.99×10^{10}	
1600	6.44×10^{11}	4.84×10^{11}	4.94×10^{11}	5.17×10^{11}		1.23×10^{11}	9.27×10^{10}	9.41×10^{10}	9.76×10^{10}	
1700	1.05×10^{12}	7.89×10^{11}	8.01×10^{11}	8.37×10^{11}		1.70×10^{11}	1.28×10^{11}	1.29×10^{11}	1.32×10^{11}	
1800	1.64×10^{12}	1.23×10^{12}	1.25×10^{12}	1.29×10^{12}		2.29×10^{11}	1.71×10^{11}	1.72×10^{11}	1.76×10^{11}	
1900	2.48×10^{12}	1.85×10^{12}	1.86×10^{12}	1.93×10^{12}		3.00×10^{11}	2.25×10^{11}	2.25×10^{11}	2.31×10^{11}	
2000	3.60×10^{12}	2.69×10^{12}	2.70×10^{12}	2.78×10^{12}		3.88×10^{11}	2.89×10^{11}	2.90×10^{11}	2.96×10^{11}	

^a Experimental values calculated by the rate constant expression in ref 2.

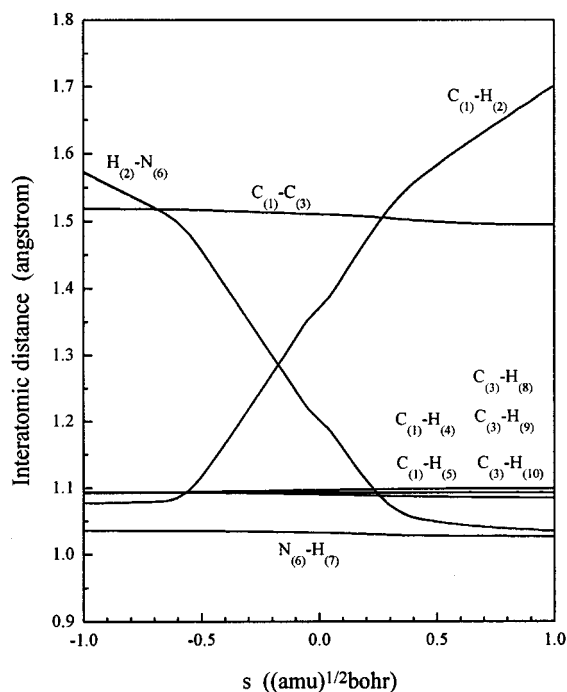


Figure 8. Changes of bond lengths (in Å) of reaction 2 as a function of *s* at the UMP2/6-311G** level.

the vibrational transformation from the $C_{(1)}-H_{(2)}$ stretching to the $H_{(2)}-N_{(6)}$ stretching takes place in the range $[-0.35, 0.0]$ along *s*. In addition, the depth of the frequency valley that the vibrational mode 17 undergoes is about 1500 cm^{-1} , and the width of the frequency valley is the region from about $s = -0.7$ to $0.8 \text{ amu}^{1/2} \text{ bohr}$ on the IRC. These dynamical properties are obviously similar to those of reaction 1.

The canonical variational transition-state theory rate constants with a small curvature tunneling correction for reaction 2 were

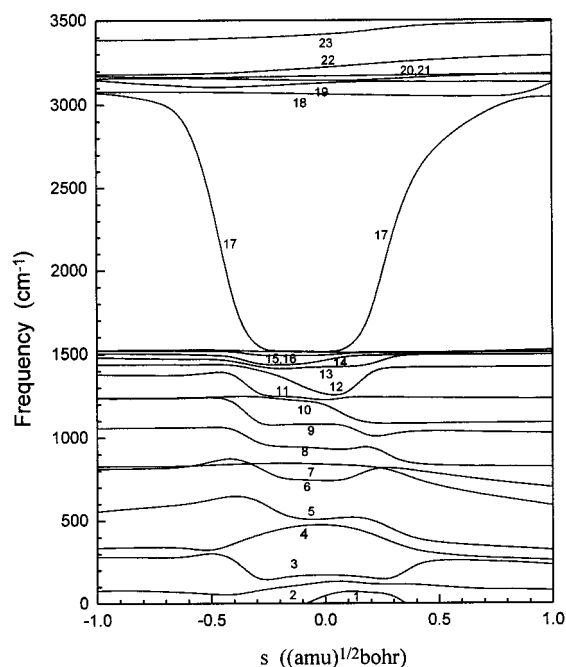


Figure 9. Generalized normal-mode vibrational frequencies of reaction 2 as a function of *s*.

calculated in a wide temperature range from 300 to 2000 K at the G2//UMP2/6-311G** level. The location of the variational transition state of the forward reaction ranges from $0.0527 \text{ amu}^{1/2} \text{ bohr}$ at 500 K to $0.0739 \text{ amu}^{1/2} \text{ bohr}$ at 2000 K, and that of the reverse reaction distributes from $0.0530 \text{ amu}^{1/2} \text{ bohr}$ at 500 K to $0.0731 \text{ amu}^{1/2} \text{ bohr}$ at 2000 K. The variational effect for reaction 2 is larger than that for reaction 1. From Table 8, we can see that the tunneling and curvature effects of the reaction path have a greater influence on the rate constants only in the lower temperature range. For the forward and reverse

reactions, the CVT/SCT rate constants are all within the range of the uncertainty of the experimental values in the measured temperature range from 1000 to 1200 K, though they are somewhat less than the experimental values. Therefore, the CVT/SCT method may also be expected to be able to afford reliable rate constants for reaction 2 in the wider temperature range. The change of the forward rate constants along the reciprocal of temperature T is drawn in Figure 5. Because the forward rate constant is only $8.94 \text{ cm}^3 \text{ mol}^{-1} \text{ s}^{-1}$ at 300 K, reaction 2 will happen very slowly at room temperature, too. Compared with the forward rate constants, the reverse reaction may take place much easier at the lower temperatures. However, at the higher temperatures. The forward rate constants are about an order of magnitude larger than the reverse reaction ones.

Conclusions

From the above discussions for reaction 1 and reaction 2, we can obtain the following conclusions.

At the G2//UMP2/6-311G** level of theory, the forward and reverse potential barriers for reaction 1 are predicted to be 91.0 and 40.2 kJ/mol, respectively, and for reaction 2 to be 74.3 and 38.9 kJ/mol, respectively. The reaction enthalpies calculated at the G2//UMP2/6-311G** level of theory for reactions 1 and 2 are 52.4 and 38.3 kJ/mol, respectively, which are slightly greater than the values in ref 2.

The changes of the generalized normal-mode vibrational frequencies along the IRC show that the "key mode" of each hydrogen-abstraction reaction describes practically the process abstracting the hydrogen atom from $\text{C}_{(1)}$ to $\text{N}_{(6)}$. The frequency change of the key mode undergoes a deep valley of frequency along the reaction coordinate, and the width of the valley corresponds essentially to the reactive region of the bond breaking and bond forming.

The CVT/SCT rate constants of the forward and reverse reactions for both reaction 1 and reaction 2 are all in good agreement with the experimental ones in the measured temperature ranges. So we could reasonably infer that the rate constants of these hydrogen-abstraction reactions calculated by the CVT/SCT method at the G2//UMP2/6-311G** level are credible for a wide temperature range from 300 to 2000 K. The tunneling effect is very important to the rate constant calculations for both reactions in the lower temperature range. The variational effect for reaction 2 is larger than for reaction 1. By comparison of reaction 1 and reaction 2, at the temperatures 500, 1000, 1500,

and 2000 K, the forward rate constants of reaction 2 are about 8, 3, 2, and 1.5 times those of reaction 1, respectively, and the reverse rate constants of reaction 2 are about factors of 10, 5.8, 5.4, and 5.2 lower than the results of reaction 1, respectively.

Acknowledgment. This work was supported by the National Natural Science Foundation of China

References and Notes

- (1) Miller, J. A.; Bowman, C. T. *Prog. Energy Combust. Sci.* **1989**, *15*, 287.
- (2) Rörig, M.; Wagner, H. G. *Ber. Bunsen-Ges. Phys. Chem.* **1994**, *98*, 858.
- (3) Hehre, W. J.; Radom, L.; Schleyer, P. V. R.; Pople, J. A. *Ab Initio Molecular Orbital Theory*; Wiley: New York, 1986.
- (4) Pople, J. A.; Head-Gordon, M.; Raghavachari, K. *J. Chem. Phys.* **1987**, *87*, 5968.
- (5) Curtiss, L. A.; Raghavachari, L.; Trucks, G. W.; Pople, J. A. *J. Chem. Phys.* **1991**, *94*, 7221.
- (6) Durant, J. L., Jr.; Rohlfing, C. M. *J. Chem. Phys.* **1993**, *98*, 8031.
- (7) Fukui, K. *J. Phys. Chem.* **1970**, *74*, 4161.
- (8) Gonzalez, C.; Schlegel, H. B. *J. Phys. Chem.* **1989**, *90*, 2154.
- (9) Gonzalez, C.; Schlegel, H. B. *J. Phys. Chem.* **1990**, *94*, 5523.
- (10) Frisch, M. J.; Trucks, G. W.; Schlegel, H. B.; Gill, P. M. W.; B. Johnson, B. G.; Robb, M. A.; Cheeseman, J. R.; Keith, T.; Petersson, G. A.; Montgomery, J. A.; Raghavachari, K.; Al-Laham, M. A.; Zakrzewski, V. G.; Ortiz, J. V.; Foresman, J. B.; Cioslowski, J.; Stefanov, B. B.; Nanayakkara, A.; Challacombe, M.; Peng, C. Y.; Ayala, P. Y.; Chen, W.; Wong, M. W.; Andres, J. L.; Replogle, E. S.; Gomperts, R.; Martin, R. L.; Fox, D. J.; Binkley, J. S.; Defrees, D. J.; Baker, J.; Stewart, J. P.; Head-Gordon, M.; Gonzalez, C.; Pople, J. A. *GAUSSIAN 94, Revision E.1*; Gaussian, Inc.: Pittsburgh, PA, 1995.
- (11) Keck, J. C. *J. Chem. Phys.* **1960**, *32*, 1035.
- (12) Garrett, B. C.; Truhlar, D. G. *J. Chem. Phys.* **1979**, *70*, 1593.
- (13) Truhlar, D. G.; Garrett, B. C. *Acc. Chem. Res.* **1980**, *13*, 440.
- (14) Truhlar, D. G.; Isaacson, A. D.; Garrett, B. C. In *Theory of Chemical Reaction Dynamics*; Baer, M., Ed.; CRC Press: Boca Raton, FL, 1985; p 65.
- (15) Steckler, R.; Chuang, Y.-Y.; Fast, P. L.; Corchado, J. C.; Coitino, E. L.; Hu, W.-P.; Liu, Y.-P.; Lynch, G. C.; Nguyen, K.; Jackels, C. F.; Gu, M. Z.; Rossi, I.; Clayton, S.; Melissas, V.; Garrett, B. C.; Isaacson, A. D.; Truhlar, D. G. *POLYRATE version 7.4*, University of Minnesota, MN, 1997.
- (16) Truhlar, D. G.; Kuppermann, A. *J. Chem. Phys.* **1970**, *52*, 3842.
- (17) Garrett, B. C.; Truhlar, D. G.; Grev, R. S.; Magnuson, A. W. *J. Phys. Chem.* **1980**, *84*, 1730.
- (18) Lu, D.-h.; Truong, T. N.; Melissas, V. S.; Lynch, G. C.; Liu, Y.-P.; Garrett, B. C.; Steckler, R.; Isaacson, A. D.; Rai, S. N.; Hancock, G.; Lauderdale, J. G.; Joseph, T.; Truhlar, D. G. *Comput. Phys. Commun.* **1992**, *71*, 235.
- (19) Liu, Y.-P.; Lynch, G. C.; Truong, T. N.; Lu, D.-h.; Truhlar, D. G. *J. Am. Chem. Soc.* **1993**, *115*, 2408.
- (20) Harmony, M. D.; Laurie, V. W.; Kuczukowski, R. L.; Schwendeman, R. H.; Ramsay, D. A.; Lovas, F. J.; Lafferty, W. J.; Maki, A. G. *J. Phys. Chem. Ref. Data* **1979**, *8*, 619.
- (21) Harmony, M. D. *J. Chem. Phys.* **1990**, *93*, 7522.